PAN

Opto-Electronics Review

journal homepage: https://journals.pan.pl/opelre

Study of the optical rotatory of potassium titanyl phosphate using the advanced dual-wavelength polarimetric method

Mykola Shopa[1*], Nazar Ftomyn[2], Yaroslav Shopa[3]

[1] Department of Atomic, Molecular and Optical Physics, Gdańsk University of Technology, ul. Narutowicza 11/12, Gdańsk 80-233, Poland
[2] Faculty of Physics, Ivan Franko National University of Lviv, Kyrylo & Mephodiy 8, Lviv 79005, Ukraine
[3] Faculty of Mathematics and Natural Sciences, Cardinal Stefan Wyszynski University in Warsaw, ul. Wóycickiego 1/3, Warsaw 01-938, Poland

Article info

Article history:
Received 12 Aug. 2024
Received in revised form 23 Sep. 2024
Accepted 24 Sep. 2024
Available on-line 19 Nov. 2024

Keywords:
polarimetry;
dual-wavelength;
crystal optics;
birefringence;
optical activity.

Abstract

A dual-wavelength high-accuracy universal polarimeter was applied to the circular birefringence and optical activity measurement in potassium titanyl phosphate (KTP) nonlinear crystal. The experimental setup used two single-mode He-Ne lasers with close wavelengths of 594 and 633 nm as light sources. Measurement has been carried out for two crystal settings in directions of a 45-degree relative angle to the [100] and [010] crystallographic axes. Multiple light reflections inside the crystal sample were considered when processing the results of the polarimetric measurements. The results have been analysed using the optical transmission function for the polariser-sample-analyser system, and 2D intensity contour maps made it possible to determine the phase parameters, systematic errors, and eigenwaves ellipticity. It was found that the gyration tensor component of the KTP crystal is equal to $g_{12} = 1.4 \cdot 10^{-5}$ which in terms of optical rotatory power corresponds to the very small magnitude of the rotation value of 2.3 deg/mm.

1. Introduction

Potassium titanyl phosphate, $KTiOPO_4$ (KTP), is a well-known material for various applications in nonlinear optics [1, 2]. KTP is a non-enantiomorphous (achiral) biaxial crystal from the mm2 point group symmetry, in which optical activity (OA) is possible, but there are no two mirror-image forms, left and right-handed crystals [3]. OA in KTP crystal can be observed only against the background of linear birefringence (LB). Therefore, the light wave splits into two elliptically polarised orthogonal components propagating at different velocities [4]. The common ellipticity k of the polarisation ellipses (the ratio of the minor to the major axis) is the same for each component and depends on the relationship between LB and circular birefringence (CB) [5]. In birefringent directions, the ellipticity k often does not exceed 10^{-3}, and CB is of the order of 10^{-5}, which creates certain difficulties for measuring OA for such light propagation directions.

Nevertheless, the interaction of light with nonlinear crystals cannot be fully described without taking the anisotropy of OA into account. Minor changes in wave fronts caused by CB should be important when calculating the phase-matching direction of the second harmonic generation (SHG). This problem was studied in detail [6–8] and for KTP exclusively [9] since most nonlinear crystals are simultaneously optically active [10]. A large group of such nonlinear materials belongs to the non-enantiomorphic mm2 class, besides KTP this includes $KTiOAsO_4$ (KTA), $RbTiOPO_4$ (RTP), $RbTiAsPO_4$ (RTA) [11–13], and other isostructural to KTP crystals [14]. Therefore, for the complete characterisation of these crystals, it is crucial to determine the exact value of OA which has certain discrepancies in the estimates of the optical rotatory power, from 20 deg/mm [15, 16] to almost 1000 deg/mm [17]. In general, these data indicate the large optical activity of KTP which is close to or even significantly higher than compared to quartz.

A significant part of the OA measurements in the presence of LB was performed by a high-accuracy universal polarimeter (HAUP) [18] and its modifications [15, 19, 20]. Various methods of measuring small changes in light polarisation exist, including those that do not use moving elements in optical schemes [21, 22]. However, this is

*Corresponding author at: mykola.shopa@pg.edu.pl

https://doi.org/10.24425/10.24425/opelre.2024.152682
1896-3757/ Association of Polish Electrical Engineers (SEP) and Polish Academic of Sciences (PAS). Published by PAS

achieved by increasing the number of polarimeter elements, such as a photoelastic modulator, and the question of their quality and influence on the measurement results arises.

From the measurement of OA anisotropy, one can also obtain information for crystallography, since the values and signs of the optical rotation can differ significantly for different directions of light propagation. Thus, according to the symmetry conditions for the mm2 class, the optical rotation in [110] and $[\bar{1}10]$ -directions should have the same absolute value, but opposite signs. Finding other ways to identify crystallographic directions based only on crystal-optical methods is not easy.

2. Setup and samples

In order to measure the OA of the KTP crystal, we used a dual-wavelength high-accuracy universal polarimeter (DHAUP) [23, 24], one of several extensions of the well-tested HAUP. All experiments have been performed using the polariser-sample-analyser (PSA) scheme. Both the polariser and the analyser were double Glan-Taylor calcite polarisers with a clear aperture of 12 × 12 mm^2. Compared to the standard polarising prism designs, the double air-gap prism provides the lowest residual ellipticity for laser beams, guarantees an extinction ratio over 100 000:1, and has a symmetric field of view [25]. The angular resolution of the motorised rotation polariser mounts with stepper motors was approximately 10^{-3} deg over the 10 deg range. According to the principles of high-accuracy polarimetry, we took into account the residual light ellipticities for the polariser p and analyser a, which can be near to the eigenwaves ellipticity k.

The dual-wavelength scheme simplifies the procedure for removing the systematic errors of the polarisation system. Previously, DHAUP was to measure the OA of the potassium dihydrogen phosphate (KDP) [26] and lithium triborate (LBO) [27] nonlinear crystals, using a gas He-Ne laser and a semiconductor laser diode. At the same time, in the case of the KTP crystal, the value of LB is much larger, so the requirements for the wavelength stability of the lasers are significantly higher. Even with a small thickness of the sample, conventional laser diodes do not provide sufficient monochromaticity and, therefore, the stability of the measured phase retardation values of the transmitted light. At the same time, two He-Ne lasers can be selected that typically exhibit a few-mode oscillation in the narrow gain bandwidth and can work with an excellent single-mode Gaussian beam quality.

In our dual-wavelength polarimeter, two He-Ne lasers with wavelengths $\lambda_1 = 594$ nm and $\lambda_2 = 633$ nm and a power of 3 and 5 mW, respectively, were alternately switched, so that for each temperature of the crystal, the necessary measurements of the transmitted light intensity were performed as a function of the angle azimuths of polariser θ and analyser χ. The analyser azimuth χ was counted from the initially crossed with the polariser position, which was chosen as the origin point, i.e., $\theta = \chi = 0$. Still, the azimuth of the polariser θ was always calculated from the principal axes and did not exceed ± 1 degree.

In high-accuracy polarimetry, the quality of crystals, often sources of additional systematic errors, is critical. The commercial KTP single crystal produced by EKSMA Optics, designed for type 2 SHG 1064 nm (phase-matching $\Theta = 90°$, $\phi = 23.5°$) was used. According to the manufacturer's data, KTP crystals are monodomain, highly homogeneous, and transparent in the 350–4400 nm range. This indicates the absence of absorption, hence even weaker dichroism in the visible range. Therefore, the uncertainty associated with the imperfection of the crystals is minimal in our case.

We started with a KTP crystal plate whose optic axis is perpendicular to the surface. The conoscopic image analysis of this plate between the crossed polariser and analyser in monochromatic and white light (Fig. 1) does not show optical rotation. This corresponds to the condition when both optic axes lie in the plane of symmetry. Under these conditions, crystallographic and dielectric (optical) coordinate systems in the KTP crystal coincide. Due to the dispersion, the angle between the optic axes grows with a decreasing wavelength (see the right panel in Fig. 1), which allows to correctly identify the direction of the z-axis.

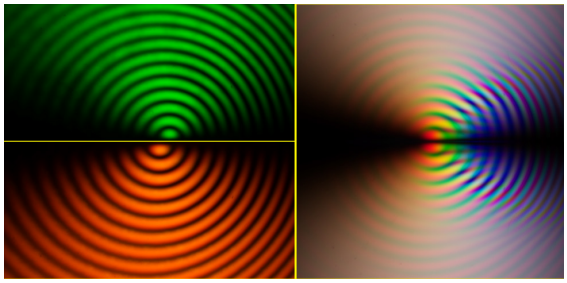

Fig. 1. Conoscopic interference patterns of a 0.54 mm thick KTP biaxial crystal plate viewed along one of its two optic axes on an Eclipse LV100N Pol polarising microscope. Two cropped and superimposed side-by-side images were obtained using green (546 nm) and yellow (589 nm) illumination (left). The dispersion of the angle between the optic axes is clearly visible also if white light illumination is used (right).

The sample for OA measurements was cut in the plane perpendicular to the direction, which is a 45-degree angle to [100]- and [010]-directions in the (001)-plane. The LB value ($\Delta n = n_z - n_{45}$) in the direction of light propagation is equal to 0.0993 for ambient condition and the average for two laser wavelengths [1, 28], therefore, a plate with a relatively small thickness $d = 182$ μm have been prepared. Measurement was carried out in the temperature interval from 295 to 360 K, i.e., which is significantly less than in Ref. 15, and the temperature changes of the phase differences $\Gamma_{1,2} = 2\pi\Delta n_{1,2} d/\lambda_{1,2}$ for each wavelength did not exceed $\Delta\Gamma < \pi/2$. It is obvious that $\Gamma_{1,2}$ contains a certain number of 2π cycles and the tested sample is not a first-order phase plate, but theoretically this does not affect the measurement results. By altering the thickness d of the sample, we achieved the condition that the $\Gamma_{1,2}$ values were not close to 0 or π, since these areas are unfavourable for data processing, and also so that $\Delta\Gamma = \Gamma_1 - \Gamma_2 \approx \pi$.

The refractive indices of the KTP crystal are relatively large, their average value for the wavelengths λ_1 and λ_2 is $\bar{n} \approx 1.821$, so the measurement data are affected by multiple light reflections (MLR) in the sample. The scalar factor that takes MLR into account for a crystal plate with the thickness d contains reflectance r_0 from Fresnel's equation and phase difference $\varphi = 4\pi\bar{n}d/\lambda$ and can be written as [29]:

$$\left(\frac{\overline{n}-1}{\overline{n}+1}\right)^2 \cos\varphi = r_0^2 \cos\varphi. \quad (1)$$

A change in the temperature of the KTP crystal is accompanied by thermal expansion and changes in the refractive index, which leads to oscillations of this factor with an amplitude of r_0^2. It follows from Ref. 30 that the values of φ and Γ increase linearly in the temperature range up to 50 K.

3. Measurement method

3.1. Transmission of the PSA system

Taking MLR into account in HAUP-like methods leads to an increase in the number of parameters and a complication of the basic relationship. The authors of Refs. 31–33 solved this problem, but the formulas for correcting the experimental results are somewhat different. Neglecting the MLR in polarimetry is believed to lead to an error, so assessing whether these corrections are correct is difficult. The authors' previous studies also concerned adapting the high-accuracy polarimetric method for determining optical anisotropy parameters in the presence of MLR [24]. By taking into account the defined values above, for small azimuths of polarisers $\theta, \chi \ll 1$, neglecting the terms containing r_0^4, $k^2, r_0 k, pk, ak$, etc., the relative light intensity $J(\theta, \chi)$of the PSA system can be reduced to the next biquadratic transmission function:

$$J(\theta,\chi) = \frac{\theta^2}{A} - 2\theta\chi\frac{\cos\Gamma - 2r_0^2\cos\varphi}{AB} + \frac{\chi^2}{B} + 2\theta\left(\frac{a\sin\Gamma}{AB} + kC\right) + 2\chi\left(\frac{p\sin\Gamma}{AB} - kD\right) + \text{const}, \quad (2)$$

where the following functions, that depend on the phase values Γ and φ, are used:

$$A(\Gamma,\varphi) = 1 - 2r_0^2\cos(\varphi-\Gamma) = 1 - 2r_0^2(\cos\varphi\cos\Gamma + \sin\varphi\sin\Gamma),$$

$$B(\Gamma,\varphi) = 1 - 2r_0^2\cos(\varphi+\Gamma) = 1 - 2r_0^2(\cos\varphi\cos\Gamma - \sin\varphi\sin\Gamma),$$

$$C(\Gamma,\varphi) = \frac{1}{A^2B}\left[\left(1-2r_0^2\cos\varphi\right)\sin\Gamma - 4r_0^2\sin\frac{\Gamma}{2}\cos\Gamma\cos\left(\varphi-\frac{\Gamma}{2}\right)\right], \quad (3)$$

$$D(\Gamma,\varphi) = \frac{1}{AB^2}\left[\left(1-2r_0^2\cos\varphi\right)\sin\Gamma - 4r_0^2\sin\frac{\Gamma}{2}\cos\Gamma\cos\left(\varphi+\frac{\Gamma}{2}\right)\right].$$

It can be seen that the neglection of MLR (i.e., $r_0 = 0$) gives $A = B = 1$ and $C = D = \sin\Gamma$. We also do not further consider the constant in (2) because it does not affect experimentally measured variables. Transmission function $J(\theta, \chi)$ is slightly different compared to $J(\theta, Y)$, which is used in a conventional HAUP, where one of the variables is $Y = \chi - \theta$. But based on (2), it is more convenient for us to analyse how experimental data is affected by LB, OA, and MLR. These effects are associated with different changes in the transmission function $J(\theta, \chi)$ and can be theoretically separated from each other.

3.2. Normalization function

Initially it should be remembered that instead of $J(\theta, \chi)$ some data of the intensity value $I(\theta, \chi)$ in arbitrary units are measured in practice. After experimental data fitting, we get:

$$I(\theta,\chi) = p_1\theta^2 + p_2\theta\chi + p_3\chi^2 + p_4\theta + p_5\chi + p_6, \quad (4)$$

where $p_1, p_2, \ldots, p_6$ are the coefficients (weights) of the biquadratic intensity function in variables (θ, χ).

Considering expressions for $A(\Gamma, \varphi)$ and $B(\Gamma, \varphi)$ the authors chose the appropriate normalization function $S(\Gamma, \varphi)$ so that the true relative light intensity $J(\theta, \chi) = \frac{I(\theta,\chi)}{S(\Gamma,\varphi)}$. As a general expression for $S(\Gamma, \varphi)$ for each measurement, we used the average value of $1/p_1$ and $1/p_3$, considering the difference between $A(\Gamma, \varphi)$ and $B(\Gamma, \varphi)$ so that:

$$S(\Gamma,\varphi) = \frac{2p_1p_3}{p_1+p_3}\left(1 - 2r_0^2\cos\varphi\cos\Gamma\right). \quad (5)$$

Therefore, to consider the MLR, one should additionally look for a way to determine the values of Γ and φ included in this expression. Obviously, without the effects of MLR, the coefficients at θ^2 and χ^2 should be equal to 1 and normalization value $S = p_1 = p_3$.

3.3. Intensity maps

For data analysis, we used the intersections of the $I(\theta, \chi)$ surface with planes of equal transmitted intensities $I(\theta, \chi)$ = const that have the form of ellipses and create the 2D intensity maps (HAUP-maps) [33, 34]. Their shape is the same as for relative light intensity $J(\theta, \chi)$. As can be seen from (2), MLR leads to the rotation of the ellipses of the constant intensity with the angle of rotation ξ dependent on the difference of $A(\Gamma, \varphi)$ and $B(\Gamma, \varphi)$. It is obvious from (2) and (3) that:

$$\tan 2\xi = \frac{p_2}{p_1 - p_3} = -\frac{\cos\Gamma - 2r_0^2\cos\varphi}{2r_0^2\sin\varphi\sin\Gamma}, \quad (6)$$

where ξ is the counterclockwise angle of rotation of major axis of the HAUP map ellipse from the θ-axis. When there is no MLR, the major axes of ellipses are always tilted by $\pm 45°$ and the ratio of semi-major to semi-minor axes depends just on the phase difference Γ [24]. Therefore, significant differences in the coefficients p_1 and p_3, which are the result of data fitting to a function of two independent variables θ and χ, indicate the influence of the MLR that needs to be considered. The linear dichroism can also cause the same effect in the changes of the 2D intensity maps [34], but KTP crystal does not exhibit this property.

3.4. Coefficients p_i and two crystal sets

The intensity of light $I(\theta, \chi)$ passing through the PSA system was measured similarly to Ref. 24, by scanning with polarisers the grid of azimuths in coordinates (θ, χ), which usually has the form of a parallelogram, consists of 21×21 points and covers intervals of approximately ± 0.8 degrees from the origin point. The surface (4) fitting to experimental data gives the $p_1, p_2, \ldots, p_6$ coefficients that were further analysed, in particular calculated 2D intensity maps were calculated for a square grid.

To increase the amount of data, the two crystal sets in the PSA system were used, i.e., a 0° set when the polariser azimuth is close to the major principal axis representing the direction of the greatest symmetry (2-fold axis, i.e., z-axis) in the crystal, and a 90° set when the polariser azimuth is perpendicular do z-axis. Change from 0° set to 90° set was achieved by rotating the sample around the direction of the laser beam propagation in the polarimeter. During further data processing, we had to take into account the fact that after the 90° crystal rotation, the ellipticity k and the phase difference Γ change their signs to the opposite, and the residual ellipticity p of light after the polariser does not change.

3.5. Invariant azimuth

The main procedure of DHAUP is to find the dependence of the analyser azimuth χ that corresponds to the minimum transmission of the PSA system on the polariser azimuth θ, i.e., the $\chi_{\min}^{\mathrm{PSA}}(\theta)$ dependence. In the polariser-analyser (PA) system, this dependence is trivial $\chi_{\min}^{\mathrm{PA}}(\theta) = \theta$ and corresponds to the condition of the crossed polarisers. The rotation of the polarisers is a standard feature of the HAUP-like polarimeters. But one should consider the systematic angular error $\delta\chi$ in determination of the relative position of the polarisers after the sample is set in the PSA system. This error can also accumulate due to mechanical imperfections, especially if the experiment continues for a long time. From (2) under the condition $\left(\frac{\partial I}{\partial \chi}\right)_{\theta} = 0$, it can be concluded that:

$$\chi_{1,2\min}^{\mathrm{PSA}}(\theta) = \theta \frac{\cos\Gamma_{1,2} - 2r_0^2 \cos\varphi_{1,2}}{A_{1,2}} + kB_{1,2}D_{1,2} - \frac{p\sin\Gamma_{1,2}}{A_{1,2}} - \delta\chi, \tag{7}$$

where indices 1, 2 correspond to the values and functions for λ_1 and λ_2 laser wavelengths. At the same time, we assume that the values of k, p, r_0 and $\delta\chi$ do not depend on the temperature and the change of two close wavelengths. Despite the complexity form of the right-hand side of (7), for a constant temperature of the sample, the azimuth of the analyser $\chi_{1,2\min}^{\mathrm{PSA}}$ depends linearly on θ. $\Gamma_{1,2}$ is the basic value for the measurement data analysis, but the slope of the linear dependence (7) differs from $\cos\Gamma_{1,2}$, which can be calculated from the relation:

$$\cos\Gamma_{1,2} = A_{1,2}\frac{\partial\chi_{1,2\min}^{\mathrm{PSA}}}{\partial\theta} + 2r_0^2\cos\varphi_{1,2}. \tag{8}$$

Two polariser azimuths θ_{01} and θ_{02}, that meet the condition

$$\chi_{1,2\min}^{\mathrm{PSA}}(\theta) = \chi_{1,2\min}^{\mathrm{PA}}(\theta) \tag{9}$$

are called invariant. From the intersection point of two linear relationships $\chi(\theta)$ in PA and PSA polarisation systems, one can determine it with high accuracy. Absolute value of the polariser azimuth must start from the principal crystal axis and is initially unknown, but the start offset of the θ azimuth angle is the same for both wavelengths, so it can be easily taken into account. It is obvious that the difference of invariant azimuths $\chi_{1\min}^{\mathrm{PSA}}(\theta) - \chi_{2\min}^{\mathrm{PSA}}(\theta)$ does not contain this offset.

From (7), it is found that the difference of invariant azimuths $\Delta\theta_0 = \theta_{01} - \theta_{02}$, which are independently measured for two wavelengths, is:

$$\begin{aligned}\Delta\theta_0 = &\left(\frac{A_1B_1D_1}{A_1 - \cos\Gamma_1 + 2r_0^2\cos\varphi_1} - \frac{A_2B_2D_2}{A_2 - \cos\Gamma_2 + 2r_0^2\cos\varphi_2}\right)k \\ &-\left(\frac{\sin\Gamma_1}{A_1 - \cos\Gamma_1 + 2r_0^2\cos\varphi_1} - \frac{\sin\Gamma_2}{A_2 - \cos\Gamma_2 + 2r_0^2\cos\varphi_2}\right)p \\ &-\left(\frac{A_1}{A_1 - \cos\Gamma_1 + 2r_0^2\cos\varphi_1} - \frac{A_2}{A_2 - \cos\Gamma_2 + 2r_0^2\cos\varphi_2}\right)\delta\chi \\ &= \left(F_{k1} - F_{k2}\right)k - \left(F_{p1} - F_{p2}\right)p - \left(F_{x1} - F_{x2}\right)\delta\chi.\end{aligned} \tag{10}$$

The value of OA in this expression is determined by the ellipticity k of the eigenwaves which is included here together with the systematic errors p and $\delta\chi$. The introduced functions $F_{k1,2}(\Gamma, \varphi)$, $F_{p1,2}(\Gamma, \varphi)$ and $F_{x1,2}(\Gamma, \varphi)$ depend only on $\Gamma_{1,2}$, $\varphi_{1,2}$ and r_0^2, so they should be calculated additionally.

4. Measurement results

4.1. Intensity maps analysis

The authors performed second-order surface fitting to the measured data in Octave using the appropriate optimization package, thus obtaining the $p_1, p_2, \ldots, p_6$ coefficients. Based on the temperature dependence of the p_1 and p_3 coefficients ratio in the biquadratic $I(\theta, \chi)$ functions for 594 nm and 633 nm wavelengths, the two temperature values can be found, for which according to (2), the ratio $\frac{p_1}{p_3} = \frac{B}{A} = 1$ and correspondingly $\sin\varphi_{1,2} = 0$. For these temperatures, the phase value in the interference factor $\varphi_{1,2} = 0$ and π, respectively.

Assuming that the phase $\varphi_{1,2}$ increases linearly for a small temperature interval, we applied the linear least squares method for the 0° and 90° crystal sets. Thus, the following calculations for each temperature became possible: (i) normalization function $S(\Gamma, \varphi)$ based on the relation (5); (ii) functions $A(\Gamma, \varphi) = S(\Gamma, \varphi)/p_1$ and $B(\Gamma, \varphi) = S(\Gamma, \varphi)/p_3$; (iii) true values of $\Gamma_{1,2}$ and the corresponding trigonometric functions, which depend on the phase difference.

Figure 2 demonstrates the temperature dependencies of the functions $A(\Gamma, \varphi)$ and $B(\Gamma, \varphi)$, which are built based on experimental data for two wavelengths and calculated

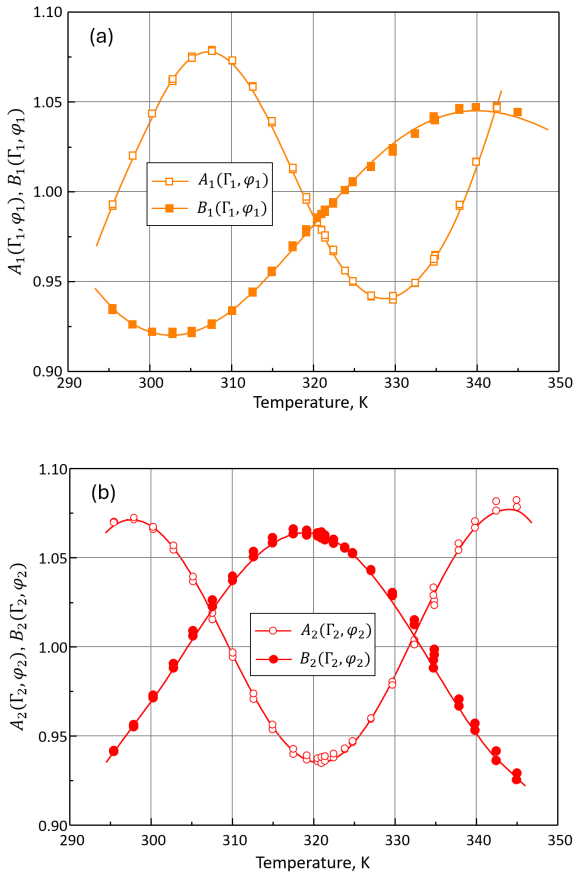

Fig. 3. Temperature dependencies of A and B normalized functions after approximation of experimental data for the 90° set of the sample and for wavelength $\lambda_1 = 594$ nm (a) and $\lambda_2 = 633$ nm (b). Graph shows both experimental data (points) and simulation (lines) based on (2).

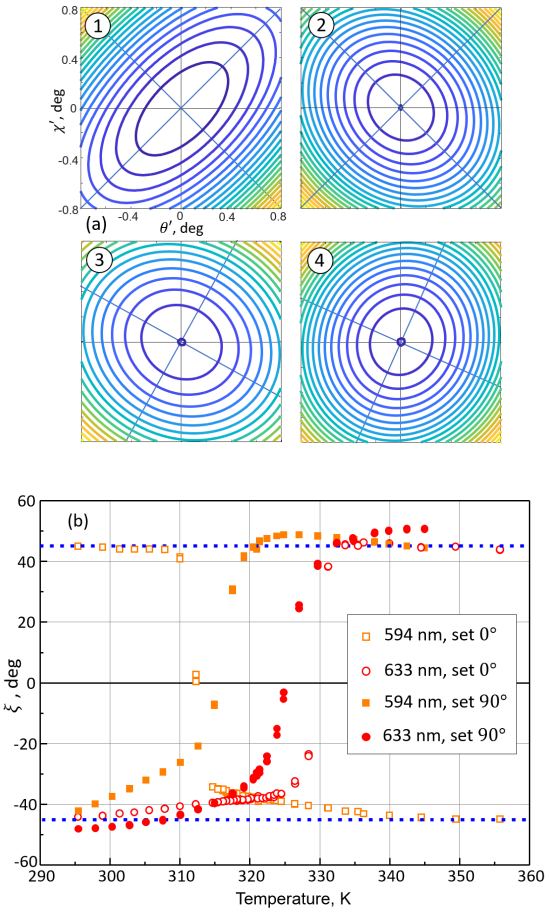

Fig. 2. Four selected 2D intensity maps obtained for the 90° set of the sample, wavelengths 594 nm (1, 3) and 633 nm (2, 4), and temperatures 342.5 K (1), 332.4 K (2), 307.6 K (3), 322.5 K (4) (a). Temperature dependencies of the angle ξ of the axis rotation of the 2D intensity map ellipse refer to the polariser azimuth θ-axis for wavelengths $\lambda_1 = 594$ nm (□, ■) and $\lambda_2 = 633$ nm (○, ●) and two crystal sets. The two blue dashed lines show angles of ± 45° (b).

according to (5). The MLR effect causes the oscillations of the functions $A(\Gamma, \varphi)$ and $B(\Gamma, \varphi)$ relative to unity with an amplitude that is significantly smaller than the expected for the KTP crystal $2r_0^2 \approx 0.17$. Apparently, the conditions of the interference in our crystal plates were not ideal, in addition, the temperature dependencies of the phase quantities Γ and φ are different, therefore, we have introduced corrections β to the interference factor so that the amplitudes of oscillations of A and B normalized functions (i.e., $\beta \cdot 2r_0^2$) correspond to the experimental values. It can be noted that the functions $A(\Gamma, \varphi)$ and $B(\Gamma, \varphi)$ are asymmetric with respect to unity and their temperature dependencies for wavelengths λ_1 and λ_2 are antiphase.

The four selected 2D intensity maps for different temperatures of the sample in the 90° set and for both wavelengths are also shown in Fig. 3. The azimuth angles of the polariser and analyser are marked here as θ' and χ', respectively because the absolute θ value must start from the principal crystal axis and is initially unknown. A close to ± 45° inclination of the major axes of the ellipses for both wavelengths (map 1 at $T = 342.5$ K and 2 at $T = 332.4$ K in Fig. 3) is visible. But at temperatures 307.6 K ($\lambda = 594$ nm) and 322.5 K ($\lambda = 633$ nm), these angles are −29.3° and −24.2°, respectively (see maps 3 and 4 in Fig. 3), which leads to a deviation in the experimentally measured phase difference $\Gamma_{1,2}$ values and transmission function $J(\theta, \chi)$ in general. Temperature dependencies of the rotation angle ξ of the 2D intensity map ellipses are shown in Fig. 3(b).

Without the effects of MLR, fitting the data to the biquadratic function (4) always gives the same coefficients ($p_1 = p_3$) and such dependence of the rotation angle on temperature has the character of a step function and only two angle values $\xi = \pm 45°$ can be observed. Significant deviation from this rule, especially for the 90° set of the sample can be observed (Fig. 3). Therefore, the 2D intensity maps in the (θ, χ) coordinates are a good indicator for the even small MLR effects in the DHAUP experiment.

4.2. *Phase differences recalculation*

Estimation of the correct temperature dependence of the phase difference Γ based on (8) is the central point of processing the polarimeter data. In these calculations, instead of the unknown values of $\cos\Gamma_{1,2}$ in (5), we initially used $\frac{\partial \chi_{1,2\min}^{\mathrm{PSA}}}{\partial \theta}$ and in the second approximation the values of $\cos\Gamma_{1,2}$ and $\Gamma_{1,2}$ have already been updated in (8). The measured temperature dependencies of the $\frac{\partial \chi_{1,2\min}^{\mathrm{PSA}}}{\partial \theta}$ differ significantly from the correct temperature dependencies of $\cos\Gamma_1$ and $\cos\Gamma_2$ calculated using the above scheme [Fig. 4(a)]. Cosine is an even function, but based on similar

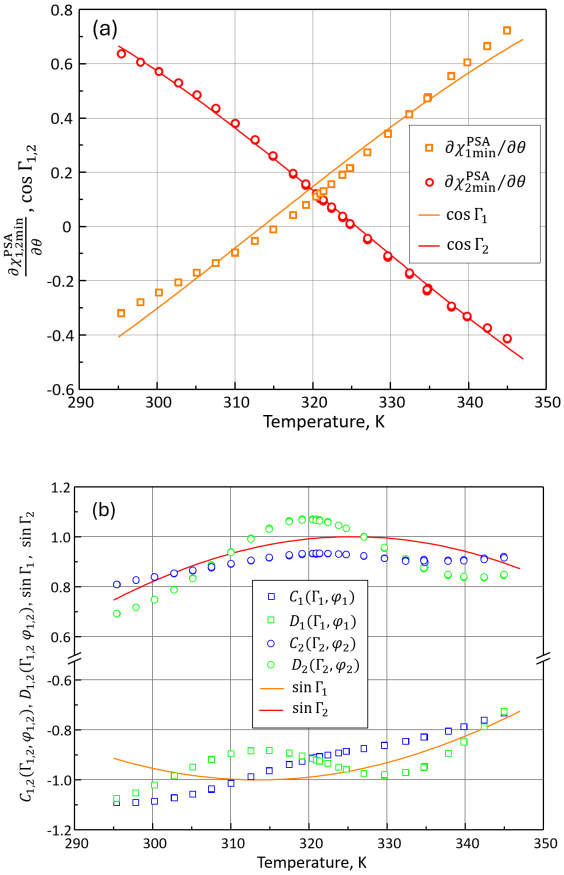

Fig. 4. Temperature dependencies of measured values of $\frac{\partial\chi^{PSA}_{1,2min}}{\partial\theta}$ (red and yellow points) for both wavelengths and recalculated functions $\cos\Gamma_{1,2}$ (solid lines) (a); $\sin\Gamma_{1,2}$ (solid line), $C_{1,2}$ (green points)m and $D_{1,2}$ (blue points) for the 90° set of the sample in the PSA system (b).

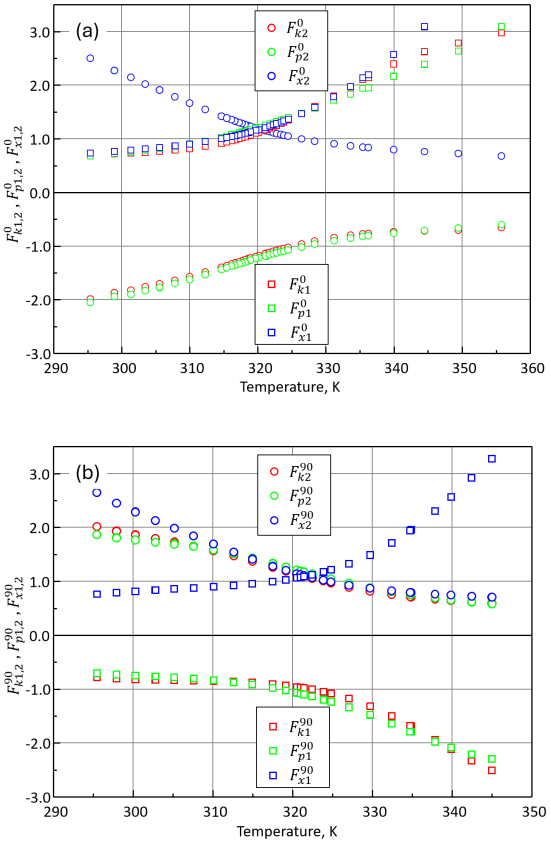

Fig. 5. Temperature dependencies of the functions differences ΔF_k (red points), ΔF_p (green points) and ΔF_x (blue points) for 0° crystal set (a) and 90° crystal set (b).

data for $\lambda_1 = 594$ nm, the different signs of the derivatives of $\cos\Gamma_1$ and $\cos\Gamma_2$ were observed. It should be assumed that the signs of $\sin\Gamma_1$ and $\sin\Gamma_2$ are opposite for both crystal sets. It is also important for other functions calculations included in transmission $J(\theta,\chi)$. In particular, the functions $C_{1,2}(\Gamma,\varphi)$ and $D_{1,2}(\Gamma,\varphi)$ for two crystal sets and for both wavelengths [Fig. 4(b)] are necessary for these calculations. In case of no MLR, these functions for each wavelength and crystal sample set become close in magnitude to $\sin\Gamma_{1,2}$ and $\frac{\partial\chi^{PSA}_{1,2min}}{\partial\theta} = \cos\Gamma_{1,2}$. Instead, one can see their significant deviation, even more, than $\frac{\partial\chi^{PSA}_{1,2min}}{\partial\theta}$ from $\cos\Gamma_{1,2}$. As follows from the transmission function (2), the functions $C_{1,2}(\Gamma,\varphi)$ and $D_{1,2}(\Gamma,\varphi)$ are the ellipticity k multipliers, therefore such significant (up to 10%) deviation from sine should be taken into account during the experiment.

Thus, using the experimentally measured values, we have calculated the functions necessary for the complete experimental data processing and the determination of the parameters related to OA.

5. Eigenwaves ellipticity and optical rotation

Neglecting the dispersion of OA in crystals for a relatively small interval of 40 nm, it is possible to remove systematic errors when measuring the small ellipticities k of optical eigenwaves. A comparison of the differences of three separate quantities included in (10) indicates that $\Delta F_k = F_{k1} - F_{k2}$ and $\Delta F_p = F_{p1} - F_{p2}$ are nearly equal (Fig. 5). This makes it possible to combine the first two terms and write (10) in the following form:

$$\Delta\theta_0 = \Delta F_k (k - p) - \Delta F_x \delta\chi. \tag{11}$$

If MLR is insignificant, then $\Delta F_k = \Delta F_p = \cot\frac{\Gamma_1}{2} - \cot\frac{\Gamma_2}{2}$ and $\Delta F_x = \frac{1}{\cos\Gamma_1} - \frac{1}{\cos\Gamma_2}$, so equation (11) is not random. Now, keeping in mind the changes in the signs of k and Γ for each of the two crystal sets (0°and 90°), we obtain the equations of two straight lines, in which $\pm k - p$ is the slope of the lines and $-\delta\chi$ is the intercept value

$$\frac{\Delta\theta_0^{0,90}}{\Delta F_x^{0,90}} = \Delta F_{kx}^{0,90}(\pm k - p) - \delta\chi, \tag{12}$$

where $\Delta F_{kx}^{0,90} = \frac{\Delta F_k^{0,90}}{\Delta F_x^{0,90}}$. This means that to determine the value of ellipticity and systematic errors, it is enough to perform a simple linear fitting.

The angular error $\delta\chi$ can be different, but we believe that the residual ellipticity p of light after the polariser is unchanged since the polariser is the first element in the PSA system and the conditions of light passing through it are unchanged after the sample is rotated by 90°. In the

dual-wavelength polarimeter, the residual ellipticity of the light after the analyser does not affect the measurement. At the same time in the conventional HAUP, it should also be considered assuming that it is constant, which is no longer so obvious.

Figure 6 shows two dependencies between the $\frac{\Delta\theta_0}{\Delta F_x}$ and $\frac{\Delta F_k}{\Delta F_x}$ values obtained for the 0° and 90° set of a 182 µm thick KTP sample, based on all previous experimental data processing considering the effects of MLR. The angular error for two different sets of the sample is sufficiently small for the high-accuracy polarimetric experiment and does not exceed $\delta\chi \approx 1.1 \cdot 10^{-3}$ deg. This indicates the good quality of the polarisation system, particularly the rotation mechanisms of the polarisers. Solid lines in Fig. 6 represent the best fits to experimental data with high Pearson's correlation coefficients ($r = 0.998$) and from their slopes, we acquired: $k - p = 0.29 \cdot 10^{-4}$ for the 0° set and $-k - p = 0.49 \cdot 10^{-4}$ for the 90° set of the sample. Therefore, the systematic error, which in the HAUP-like setup, is considered to be the residual ellipticity of the light after the polariser $p = -0.20 \cdot 10^{-4}$. A more practical parameter of polariser quality is ER, the ratio of the maximum and the minimum transmission of linearly polarised light through a linear polariser [35, 36]. Given that ER $\approx p^2$, it can be assumed that in the scheme of our polarimeter, the ER for the polariser significantly exceeds the value provided by the manufacturer. This indicates one of the essential advantages of a perfect polarisation system in HAUP, which contains a minimum of components and does not use additional phase elements, modulators, compensators, etc.

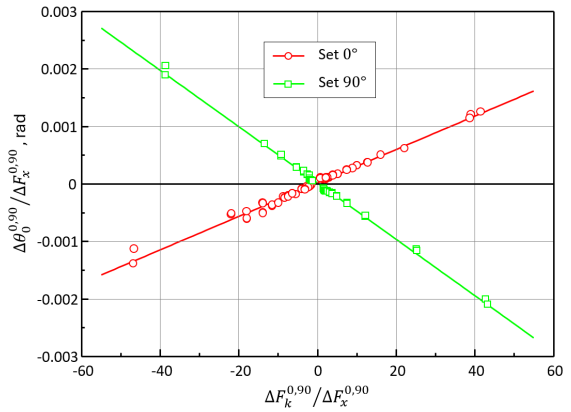

Fig. 6. The two-linear dependencies between characteristic values included in (12). Straight lines correspond to the 0° and 90° set of the sample in PSA system.

Finally, we find the ellipticity value $k = 0.39 \cdot 10^{-4}$ which is extremely small for normal waves in an optically active crystal. For directions that are not too close to an optic axis, the scalar gyration parameter (pseudoscalar parameter) is equal to $G = 2k\bar{n}\Delta n$. For the direction in xy plane with 45° to the positive direction of the x and y axes, the gyration parameter $G = g_{12}$ in the crystal with mm2 point group symmetry [5]. Thus, using the known values [37] for the average refractive index $\bar{n}$ and birefringence Δn_{45} for this direction, we have obtained $g_{12} = 1.4 \cdot 10^{-5}$ and circular birefringence $\Delta n_c = \frac{G}{\bar{n}} = 0.77 \cdot 10^{-5}$ for the wavelength interval of 594–633 nm.

6. Discussion

Even though in the KTP crystal there is no optical rotation of the polarisation plane in the direction of the optic axes, we can formally calculate the optical rotatory power (ORP) which is equal to $\rho = \frac{\pi}{\lambda\bar{n}} g_{12} = 2.3$ deg/mm. This value is significantly lower in comparison to the known data [15, 16], but similar to the ORP value for the LBO crystal [27].

Table 1 presents the main values obtained by the best fits of the experimental results obtained for a mean wavelength of 614 nm on DHAUP. Unlike the conventional HAUP, the residual ellipticity of the analyser does not affect the measurement results, so it is not presented in the table. Another advantage of our DHAUP is its insensitivity to the azimuthal error $\delta\chi$, the analog of which is the systematic error δY in Refs. 15, 18, 31, and 32.

Table 1.
Systematic errors of the polarimeter and parameters related to the optical activity of the KTP crystal for a wavelength of 614 nm. The birefringence value Δn_{45} is given according to Ref. 28.

Parameters	Values
p, 10^{-4}	−0.20(4)
$\delta\chi$, 10^{-5}	1.90(20)
Δn_{45}	0.0993
k, 10^{-4}	0.39(4)
g_{12}, 10^{-5}	1.4(2)
ρ, deg/mm	2.3(3)

Unfortunately, there is almost no detailed data on HAUP measurement in Ref. 16. The authors limited themselves to the gyration value, equivalent to an optical rotation of +22 deg/mm at 633 nm. In addition, twinning in the samples and significant circular dichroism were detected, despite the sample being rather thin (~ 30 µm). These phenomena could cause systematic errors since the crystal quality is crucial in HAUP-like experiments.

More thorough experiments measuring OA in KTP using HAUP are described in Ref. 15, in terms of optical rotation, its value is 20 deg/mm. However, there are inconsistencies between the formulas and experimental data that are not explained in this article.

Theoretical calculation of OA [17] gives a value that is not confirmed by any experimental data, since the ellipticity of eigenwaves must be at least $k \approx 0.017$ and the component of the gyration tensor $g_{12} = 6.2 \cdot 10^{-3}$. Our measurement method would definitely record such values.

Note that the conditions for measuring OA depend on the birefringence properties of the crystal. Similarly to Ref. 38, in our experiments the reliability of the gyration parameter measurement can be estimated according to the ratio $G \approx 0.2 \cdot 10^{-4} \cdot \Delta n$. This means that for a KTP crystal with $\Delta n \approx 0.1$, the minimum measurable value is $G \approx 0.2 \cdot 10^{-5}$, while in the case of a crystal with $\Delta n \approx 0.01$, it is possible to detect a value of $G \approx 0.2 \cdot 10^{-6}$. Therefore, in the crystal with the relatively large linear birefringence, an exact measurement of OA is complex, since the eigenwaves ellipticity k is smaller than systematic errors. The calculation of the optical rotation using the data of the crystal

structure based on the classical polarisation theory [39] of optical activity is complicated by the fact that the unit cell of the KTP crystal contains eight formula units and 16 lattice sites [14], moreover, the same ions are in non-equivalent positions in which their polarizabilities may differ.

7. Conclusions

We have measured the optical activity of KTP employing the dual-wavelength high-accuracy polarimeter with wavelengths of 594 and 633 nm. It was found that multiple light reflections in the sample of KTP crystal essentially affect the measured characteristic values in the high-accuracy polarimetry. This requires modifications of the basic relations, therefore the number of parameters that need to be monitored increases, and a standard HAUP-like scheme for results processing becomes complex. The dual-wavelength polarimetric method made it possible to take into account the effects of multiple light reflections on the basic functions and calculate eigenwaves ellipticity based on the measurement of only one characteristic azimuth of the polariser for each wavelength separately. Using two wavelengths made it possible to reduce the interval of temperature changes during measurements, which for a conventional HAUP at a single wavelength can be more than 100 K, increasing the likelihood of systematic errors. According to our data, the value of the optical rotation of the KTP crystal does not exceed a few degrees/mm which is significantly less than those found or calculated earlier.

Authors' statement

Research concept and design, Y.S. and N.F.; collection and assembly of data, M.S.; data analysis and interpretation, M.S. and N.F.; writing the article, Y.S., M.S., and N.F.; critical revision of the article, Y.S.; final approval of article, M.S. and Y.S.

Acknowledgements

The following funding is acknowledged: Polish Ministry Science and Higher Education (MNiSW Project 2023–2024); National Science Centre, Poland, grant no. 2021/41/B/ST3/00069.

References

[1] Bierlein, J. D. & Vanherzeele, H. Potassium titanyl phosphate: properties and new applications. *J. Opt. Soc. Am. B* **6**, 622–633 (1989). https://doi.org/10.1364/JOSAB.6.000622

[2] Zumsteg, F. C., Bierlein, J. D. & Gier, T. E. $K_xRb_{1-x}TiOPO_4$: a new nonlinear optical material. *J. Appl. Phys.* **47**, 4980–4985 (1976). https://doi.org/10.1063/1.322459

[3] Flack, H. D. Chiral and achiral crystal structures. *Helv. Chim. Acta* **86**, 905–921 (2003). https://doi.org/10.1002/hlca.200390109

[4] Yariv, A. & Yeh, P. *Optical Waves in Crystal Propagation and Control of Laser Radiation*. (Wiley, 1983).

[5] Nye, J. *Physical Properties of Crystals*. (Oxford University Press, 1985).

[6] Rabin, H. & Bey, P. P. Phase matching in harmonic generation employing optical rotatory dispersion. *Phys. Rev.* **156**, 1010–1016 (1967). https://doi.org/10.1103/PhysRev.156.1010

[7] Simon, H. J. & Bloembergen, N. Second-harmonic light generation in crystals with natural optical activity. *Phys. Rev.* **171**, 1104–1114 (1968). https://doi.org/10.1103/PhysRev.171.1104

[8] Rodriguez, V. Quantitative determination of linear and second-harmonic generation optical effective responses of achiral or chiral materials in planar structures: Theory and materials. *J. Chem. Phys.* **128**, 064707 (2008). https://doi.org/10.1063/1.2824985

[9] Tebbutt, I. J. Effect of optical activity on type-I and type-II phase matching in second-harmonic generation. *Appl. Opt.* **31**, 5810–5812 (1992). https://doi.org/10.1364/AO.31.005810

[10] Dmitriev, V. G., Gurzadyan, G. G., & Nikogosyan, D. N. *Handbook of Nonlinear Optical Crystals* (Springer, 2013).

[11] Cheng, L. K. & Bierlein, J. D. KTP and isomorphs – recent progress in device and material development. *Ferroelectrics* **142**, 209–228 (1993). https://doi.org/10.1080/00150199308237899

[12] Chani, V. I., Shimamura, K., Endo, S. & Fukuda, T. Growth of mixed crystals of the $KTiOPO_4$ (KTP) family. *J. Cryst. Growth* **171**, 472–476 (1997). https://doi.org/10.1016/S0022-0248(96)00693-8

[13] Roth, M., Tseitlin, M. & Angert, N. Composition-dependent electro-optic and nonlinear optical properties of KTP-family crystals. *Opt. Mater.* **28**, 71–76 (2006). https://doi.org/10.1016/j.optmat.2004.11.056

[14] Thomas, P. A., Mayo, S. C. & Watts, B. E. Crystal structures of RbTiOAsO4, $KTiO(P_{0.58}As_{0.42})O_4$, $RbTiOPO_4$ and $(Rb_{0.465}K_{0.535})TiOPO_4$, and analysis of pseudosymmetry in crystals of the $KTiOPO_4$ family. *Acta. Crystallogr. B.* **48**, 401–407 (1992). https://doi.org/10.1107/S0108768192002465

[15] Hernández-Rodríguez, C., Fragoso-López, A. B., Herreros-Cedrés, J. & Guerrero-Lemus, R. Temperature-dependent optical rotatory power in the presence of birefringence of KTA and KTP crystals by the high-accuracy universal polarimeter method at 632.8 nm wavelength. *J. Appl. Crystallogr.* **47**, 566–574 (2014). https://doi.org/10.1107/S1600576714000454

[16] Thomas, P A., Tebbutt, I. J. & Glazer, A. M. Potassium titanyl phosphate, $KTiOPO_4$. I. Experimental investigation of optical gyration, absolute optical chirality and twinning. *J. Appl. Crystallogr.* **24**, 963–967 (1991). https://doi.org/10.1107/s0021889891007239

[17] Sturm, C., Zviagin, V. & Grundmann, M. Dielectric tensor, optical activity, and singular optic axes of KTP in the spectral range 0.5–8.4 eV. *Phys. Rev. Mater.* **4**, 055203 (2020). https://doi.org/10.1103/PhysRevMaterials.4.055203

[18] Kobayashi, J., Asahi, T., Takahashi, S. & Glazer, A. M. Evaluation of the systematic errors of polarimetric measurements: application to measurements of the gyration tensors of α-quartz by the HAUP. *J. Appl. Crystallogr.* **21**, 479–484 (1988). https://doi.org/10.1107/S0021889888005503

[19] Takanabe, A., Koshima, H. & Asahi, T. Fast-type high-accuracy universal polarimeter using charge-coupled device spectrometer. *AIP Adv.* **7**, 025209 (2017). https://doi.org/10.1063/1.4977440

[20] Tanaka, M., Nakamura, N., Koshima, H. & Asahi, T. An application of the advanced high-accuracy universal polarimeter to the chiroptical measurement of an intercalated compound $K_4Nb_6O_{17}$ with high anisotropy. *J. Phys. D: Appl. Phys.* **45**, 175303 (2012). https://doi.org/10.1088/0022-3727/45/17/175303

[21] Arteaga, O., Freudenthal, J., Wang, B. & Kahr, B. Mueller matrix polarimetry with four photoelastic modulators: theory and calibration. *Appl. Opt.* **51**, 6805–6817 (2012). https://doi.org/10.1364/AO.51.006805

[22] Martin, A. T., Nichols, S. M., Murphy, V. L. & Kahr, B. Chiroptical anisotropy of crystals and molecules. *Chem. Comm.* **57**, 8107–8120 (2021). https://doi.org/10.1039/D1CC00991E

[23] Shopa, Y., Shopa, M. & Ftomyn, N. Dual-wavelength laser polarimeter and its performance capabilities. *Opto-Electron. Rev.* **25**, 6–9 (2017). https://doi.org/10.1016/j.opelre.2017.01.001

[24] Shopa, M., Ftomyn, N. & Shopa, Y. Dual-wavelength polarimeter application in investigations of the optical activity of a langasite crystal. *J. Opt. Soc. Am. B* **34**, 943–948 (2017). https://doi.org/10.1364/josaa.34.000943

[25] Double Glan-Taylor Polarizers. Thorlabs. https://www.thorlabs.com/catalogpages/v21/906.pdf (Accessed: July 30th, 2024).

[26] Shopa, M. *et al*. Polarimetric studies of l-arginine-doped potassium dihydrogen phosphate single crystals. *J. Appl. Crystallogr.* **53**, 1257–1265 (2020). https://doi.org/10.1107/S1600576720010870

[27] Shopa, M., Ftomyn, N. & Shopa, Y. Optical rotation in the lithium triborate nonlinear crystal. *J. Appl. Crystallogr.* **56**, 432–438 (2023). https://doi.org/10.1107/S160057672300136X

[28] Kato, K. & Takaoka, E. Sellmeier and thermo-optic dispersion formulas for KTP. *Appl. Opt.* **41**, 5040–5044 (2002). https://doi.org/10.1364/ao.41.005040

[29] Born, M. & Wolf, E. *Principles of Optics: Electromagnetic Theory of Propagation, Interference and Diffraction of Light*. (Elsevier, 2013).

[30] Emanueli, S. & Arie, A. Temperature-dependent dispersion equations for $KTiOPO_4$ and $KTiOAsO_4$. *Appl. Opt.* **42**, 6661–6665 (2003). https://doi.org/10.1364/AO.42.006661

[31] Hernández-Rodríguez, C. & Gómez-Garrido, P. Optical anisotropy of quartz in the presence of temperature-dependent multiple reflections using a high-accuracy universal polarimeter. *J. Phys. D: Appl. Phys.* **33**, 2985 (2000). https://doi.org/10.1088/0022-3727/33/22/318

[32] Gomez, P. & Hernandez, C. High-accuracy universal polarimeter measurement of optical activity and birefringence of α-quartz in the presence of multiple reflections. *J. Opt. Soc. Am. B* **15**, 1147–1154 (1998). https://doi.org/10.1364/JOSAB.15.001147

[33] Moxon, J. R. L. & Renshaw, A. R. The simultaneous measurement of optical activity and circular dichroism in birefringent linearly dichroic crystal sections. I. Introduction and description of the method. *J. Phys. Condens. Matter* **2**, 6807–6836 (1990). https://doi.org/10.1088/0953-8984/2/32/012

[34] Shopa, M. & Ftomyn, N. Application of two-dimensional intensity maps in high-accuracy polarimetry. *J. Opt. Soc. Am. A* **36**, 485–491 (2019). https://doi.org/10.1364/JOSAA.36.000485

[35] Bennett, J. M. Polarizers. in *Handbook of Optics.* (eds. Bass, M., Van Stryland, E. W., Wolfe, W. L. & Williams, D. R.) vol. 2 (McGraw-Hill, 1995).

[36] Takubo, Y., Takeda, N., Huang, J. H., Muroo, K. & Yamamoto, M. Precise measurement of the extinction ratio of a polarization analyser. *Meas. Sci. Technol.* **9**, 20–23 (1998). https://doi.org/10.1088/0957-0233/9/1/004

[37] Fan, T. Y. *et al*. Second harmonic generation and accurate index of refraction measurements in flux-grown $KTiOPO_4$. *Appl. Opt.* **26**, 2390–2394 (1987). https://doi.org/10.1364/AO.26.002390

[38] Kaminsky, W., Thomas, P. A. & Glazer, A. M. Optical rotation in $RbTiOAsO_4$ (point group mm2). *Z. Kristallogr. Cryst. Mater.* **217**, 1–7 (2002). https://doi.org/10.1524/zkri.217.1.1.20799

[39] Devarajan, V. T. & Glazer, A. M. Theory and computation of optical rotatory power in inorganic crystals. *Acta Crystallogr. A* **42**, 560–569 (1986). https://doi.org/10.1107/S0108767386098732